Measurement of isotope shifts in C12 and C13 glyoxal absorption at visible wavelengths, and first application to DOAS retrievals

Natasha R. Goss
Undergraduate Honors Thesis in Chemistry
March 14th, 2013

Thesis Advisor:
Dr. Rainer Volkamer, Department of Chemistry and Biochemistry

Defense Committee:
Dr. Rainer Volkamer, Department of Chemistry and Biochemistry
Dr. Geoff Tyndall, National Center for Atmospheric Research
Dr. Cortlandt Pierpont, Department of Chemistry and Biochemistry

Abstract

Glyoxal (CHOCHO) is an atmospheric trace gas produced by the radical-initiated oxidation of hydrocarbons. High resolution measurements of the glyoxal absorption spectrum in the visible wavelength range are needed as reference spectra to calibrate optical spectroscopic measurements of this gas. The UV-vis absorption spectra of C13-disubstituted glyoxal and ambient (C12) glyoxal were collected at moderately high (1 cm^{-1}) resolution. Isotopic shifts of up to 0.289 nm were observed at the 451-456 nm strong band, but no shifts were observed at the 438-441 nm band. The ability to differentiate between atmospheric glyoxal and $^{13}CHO^{13}CHO$ (C13 glyoxal) is assessed through spectral analysis of synthetic glyoxal spectra with added noise under various conditions, including the presence/absence of other gases that overlap the glyoxal spectral features, various forms of experimental noise and measurement resolution, and by varying the spectral window used for analysis. It is found that decreasing resolution linearly increases (R^2 >0.95) deviation from known C12 and C13 glyoxal concentrations, while varying baseline correction polynomials does not produce such a trend. Furthermore, the presence of H_2O has no significant effect on the glyoxal retrieval, while addition of NO_2 can cause ~10% deviations. These deviations border on significance: they are slightly less than 3σ of the retrieval error. It is thus concluded that the now available C13 absorption spectrum provides a means to distinguish C12 and C13 glyoxal through multispectral techniques such as cavity enhanced DOAS.

Introduction

Glyoxal (CHOCHO), the smallest alpha-dicarbonyl, is commonly formed in the atmosphere as a product of volatile organic compound (VOC) oxidation (Volkamer et al. 2005b). It is of analytical interest as an indicator of VOC photochemistry (Volkamer et al. 2007), and

measurements of carbonyls such as glyoxal may be used to test ozone formation models (Grosjean et al. 1996). Biogenic formation pathways are the largest sources of glyoxal, followed by direct anthropogenic emission and pyrogenic formation (Stavrakou et al., 2009). In addition, glyoxal may be produced by the combined O_3/OH-radical oxidation of benzene and toluene derivatives, which are often anthropogenically generated, as well as some other ring systems, alkenes, butadiene, and acetylene (Volkamer et al. 2007). Biogenic formation pathways include the atmospheric degradation of isoprene and its oxidation products such as glycolaldehyde and methyl vinyl ketone (Orlando and Tyndall 2001, Galloway 2011).

Glyoxal has multiple anthropogenic sources and industrial uses. Glyoxal is present in butter and fermented food products such as wine, cheese, and vinegar (Barros et al. 1999; Yamaguchi et al. 1994). Small amounts of glyoxal have been detected in automobile tailpipe emissions (Grosjean et al. 2001) and in cigarette and fire smoke (Kielhorn et al. 2004). In manufacturing, glyoxal is used to produce pharmaceuticals, dyes, and some synthetic fabrics. It is commercially produced by catalytic oxidation of ethylene glycol in air at elevated temperatures (Kielhorn et al. 2004).

Glyoxal is detectable in both the terrestrial (Volkamer et al. 2005a) and oceanic atmosphere (Sinreich et al. 2010). The highest glyoxal concentration observed in Mexico City is 1.2 ppb (Volkamer et al. 2005a). In other sets of urban measurements, glyoxal concentrations varied widely with an average volume mixing ratio of 0.78 ppb (Grosjean 1996). Volkamer et al. (2005 GRL) determined in a study of pollution in Mexico City that the atmospheric lifetime is 1.3 hours under direct sun, a typical lifetime for glyoxal exposed to sunlight (Atkinson 2000). Glyoxal was detected in the Marine Boundary Layer of the remote tropical Pacific Ocean using differential optical absorption spectroscopy (DOAS) (Sinreich et al. 2010). Based on known

atmospheric lifetimes, this remote-ocean glyoxal must be produced over water.

The major degradation pathway of glyoxal in the atmosphere is photolysis in sunlight, which yields H_2, CO, HCHO and HCO radicals. Photolysis determines ~66% of the gas-phase chemical loss reaction, and hydroxyl radicals account for ~33% (Volkamer et al. 2005b, Plum 1983). Glyoxal is also a source for secondary organic aerosol (SOA), although the extent to which heterogeneous uptake contributes to form SOA is currently not well known (Volkamer et al., 2007, Stavrakou et al. 2009). Minor degradation pathways include solid-state transfer: namely, dry and wet deposition. In addition, glyoxal may undergo nighttime reaction with NO_3 radicals (Plum 1983).

Gaseous C12 glyoxal is often generated by heating glyoxal trimer dihydrate crystals in the presence of P_2O_5; it may also be produced by purification from aqueous solution (Orlando 2001). Because C13 glyoxal is not commercially available in either form, it was synthesized herein from acetylene through the chlorine radical oxidation mechanism described by Yarwood et al. (1991).

A precise C13 glyoxal absorption spectrum is necessary for spectroscopic analysis methods such as DOAS. Volkamer et al. (2005) measured the spectrum of C12 glyoxal to 0.06 cm^{-1} precision in the 250–526 nm range using Fourier transform spectrometry. Good agreement was observed with the previous UV-vis and IR glyoxal spectrum studies, including Orlando et al. (2001). Previous study of the spectrum involved assignment of several absorption bands. The long-wavelength absorption band peaks at 455 nm; this peak results from a relatively strong $\tilde{A}\ ^1A_u \leftarrow \tilde{X}\ ^1A_g$ ($\pi^* \leftarrow$ n) transition to the first excited state (Chen and Zhu 2003). Larsen et al. (2003) investigated the geometry and energetic transitions of glyoxal in the IR range by comparing isotopically substituted glyoxal, including the disubstituted C13 compound. Birss et

al. (1970; 1977) provide evidence for isotopic shifts in glyoxal through their examination of bending and stretching modes in the visible range. In combination with deuterated and ^{18}O enriched forms of glyoxal, C13 glyoxal has been used to determine the geometry of the glyoxal molecule (Birss et al. 1977). However, their work does not provide a quantitative cross-section, which is required for the DOAS method.

Substitution of the carbonyl carbons in glyoxal with C13 produces an isotopically enriched compound with different ro-vibrational levels and a shifted UV-vis spectrum. Although the presence of two C13 atoms in the same small molecule is statistically very rare in nature, C13 glyoxal may be prepared in the laboratory using an enriched carbon skeleton, then used as an experimental tracer. Spectroscopic detection of C13 glyoxal in the UV-vis region requires a high-resolution reference spectrum. To intelligently employ the spectrum in laboratory analyses, cross-correlation between the C13 spectrum and that of C12 glyoxal must be carefully noted under a variety of simulated instrumental conditions. These conditions include varying types of instrument noise and noise produced by spectrum parameters such as a baseline correction polynomial.

Experimental Section

Collection of High-Resolution Spectra

Because C13 glyoxal is not commercially available, glyoxal was synthesized through the chlorine-initiated oxidation of acetylene in the presence of excess oxygen and nitrogen at 1 atm total pressure as described by Yarwood et al. (1991) (Figure 1).

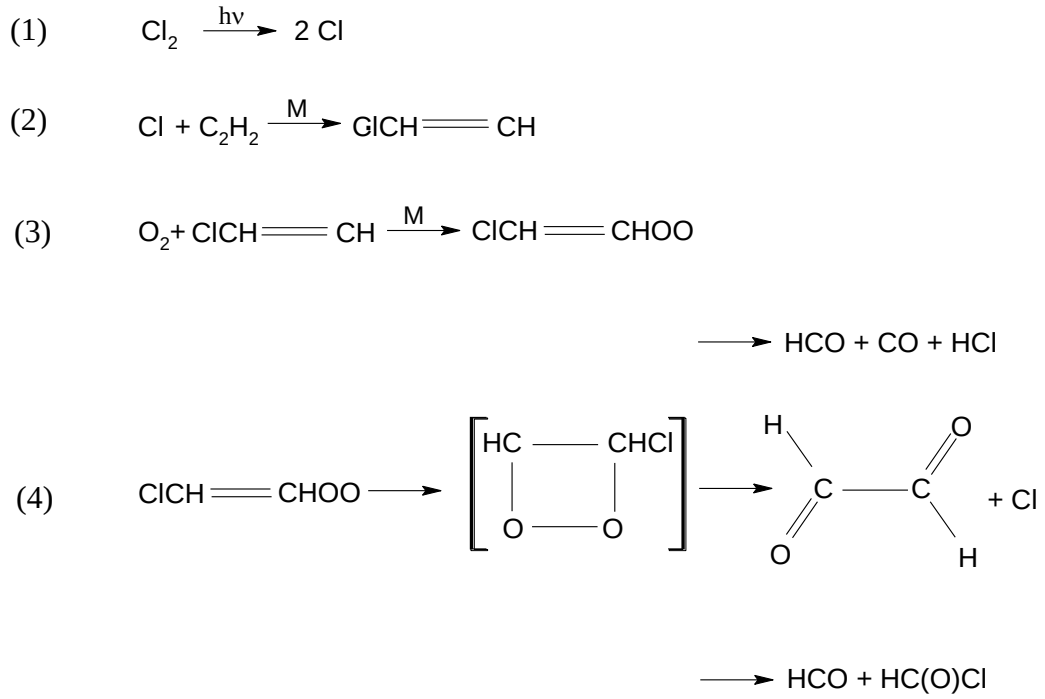

Figure 1: Mechanism of chlorine-radical-initiated formation of glyoxal. The glyoxal pathway is followed 21% of the time (Yarwood et al. 1991).

The chlorine radicals were produced from UV-photolysis of chlorine in a small reaction vessel. The signal-to-noise ratio of glyoxal was optimized for collection of a moderately high resolution (1 cm^{-1}) UV-vis spectrum. Analyte concentration and stable lifetime were the primary factors influencing the signal-to-noise ratio. In initial tests, glyoxal production was monitored using a low-resolution OceanOptics spectrophotometer. Reaction parameters including optimal photolysis lamp filtration, reactant concentrations, and flow cell surface-area-to-volume ratio were examined. Under the final protocol, glyoxal lifetime limited S/N. The optical density was most sensitive to varying chlorine and to a lesser degree to varying acetylene concentrations.

Final spectra using optimized concentration parameters were collected at 1 cm^{-1} resolution with boxcar apodization by means of a Bruker 120 HR FTS using an external instrument port, a light-emitting diode (centered at 459 nm, FWHM 27 nm), and a UV blacklamp for photolysis (Figure 2). During these experiments, 3 torr chlorine, 80 torr acetylene, 150 torr

oxygen, and 400 torr nitrogen were introduced to the manifold. To conserve C13 acetylene while using a standard manifold, C13 acetylene was added to the cell first, then the excess drawn off into the original vessel using a liquid nitrogen trap. Exposure of the mixture to UV light in a 1.00 m gas cell yielded glyoxal optical densities on the order of 10% at $1cm^{-1}$ optical resolution.

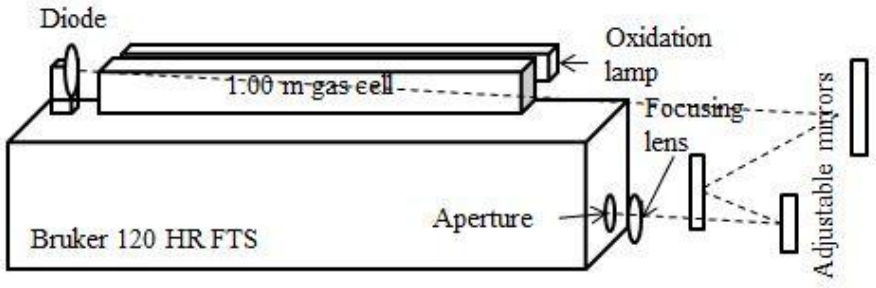

Figure 2: The Bruker 120 HR FTS external port arrangement.

Continued resupply of glyoxal sustained elevated glyoxal levels over a period of ~5 hrs. Wall loss and photolytic degradation were the major pathways for glyoxal elimination. Before collecting sample spectra, a one-hour reference spectrum was taken with a cell containing nitrogen at atmospheric pressure. Each sample spectrum was collected in one-hour segments. After each segment, the spectrum was examined to determine whether glyoxal was still present. When the amount of glyoxal had substantially diminished, collection ceased and a second one-hour reference was collected. Segments were averaged and the averaged intervals converted to standard absorption spectra using Beer's Law:

$$A = \ln\left(\frac{I_0}{I}\right) = \sigma\, c\ \ l \qquad (1)$$

The average of the reference spectra was taken to be I_0. The absorption spectra thus obtained were converted from an optical density to a cross-section, independent of pathlength or concentration. The amount of C12 glyoxal was determined using the Volkamer et al. (2005) cross-section as a reference fit between 430 and 475 nm. The same fitting procedure was

performed on C13 glyoxal under spectral shift and second-order stretch parameters that accounted for isotopic effects.

Baseline Correction of Spectra

The diode (centered at 459 nm, FWHM 27 nm) used as a light source in spectrum collection exhibited drift, causing the C12 and C13 spectra to have nonlinear baselines. The method developed by Volkamer et al. (2005) (V05) was adapted to correct for baseline drift in the LED. First, the slant column density of glyoxal was determined through polynomial fitting of the C12 and C13 spectra to the V05 spectrum. Spectra were convoluted to a common (0.3 nm) resolution sufficient to capture major spectral features, and second-order shift and stretch fitting accounted for isotopic distortions to the locations of C13 absorption peaks. Second, the C12 and V05 cross section integrals were compared over fixed 50 cm^{-1} intervals. Third, a 5^{th}-order polynomial was fit to the series of integral differences. Finally, the fifth-order polynomial was subtracted from the C12 spectrum to produce a corrected absorption spectrum.

A similar process was followed to correct the C13 spectrum. First, spectral stretching and shifting were used to match the absorption peaks of the C12 and C13 spectra, providing a flat-baseline approximation of the C13 spectrum. However, isotope shifts in spectral features caused absorption differences to remain between the stretched C12 baseline approximation and the C13 spectrum. These differences were actively accounted for by including only points from wavelengths where no significant glyoxal absorption is observed to determine the polynomial. A 2^{nd} order polynomial was fit to the regions of low absorption and the integral correction performed as above. Corrected spectra spanned 23250-21250 cm-1 (430-470 nm) for both C12 and C13.

To ensure that the final integral cross section remained consistent between the C12 and

C13 cross section spectra, both spectra were converted to 0.3nm FWHM optical resolution. The C13 cross section was fit to the C12 spectrum allowing for a second-order stretch and squeeze of the wavelength stamp. A fit factor of unity would indicate that their integrals do not differ. The observed fit factor was 1.01, indicating that the calibration from the C12 spectrum (V05) was indeed successfully transferred to calibrate the C13 absorption cross section spectrum.

Parameter Testing and Analysis of Synthetic Spectra

Given the similarity between the C12 and C13 cross section spectra, we have performed sensitivity studies to evaluate the potential for cross-talk, or interference, between the spectra in a DOAS retrieval. Analysis of synthetic spectra can aid in determining whether C13 and C12 inputs may be differentiated and provide a guide to uncertainties in this differentiation. Synthetic spectra containing known amounts of C12 and C13 glyoxal were produced, as were spectra containing mixtures of both isotopic forms in the presence and absence of water and NO_2. The range of parameters evaluated is summarized in Table 1 and includes spectrum resolution, baseline correction polynomial order, type of noise structure, and the presence of other gases in the spectrum.

The concentrations of the various compounds in synthetic spectra were determined using Windoas 2.1, a DOAS analysis program. DOAS uses absorption across a range of wavelengths to simultaneously detect the presence of multiple atmospheric gases. The chemical fingerprints of known molecular cross sections are compared to an absorption spectrum, yielding a slant column measurement. A slant column measurement is the abundance of a particular gas along an atmospheric light path.

The effect of different forms of instrument noise was assessed. We generated four different types of noise using two different random noise spectra (A and B) as starting points,

leading to a total of eight noise forms. The four types of noise were: white noise alone, a combination of white noise and the result of its Gaussian-convolution at 0.2 nm, the Gaussian noise at 0.7 nm, and triangular noise created through low-pass binomial filtration. Two randomized white noise series (Gaussian distributions; RMS = 1E-4) were generated. To create the Gaussian-convoluted noise, a white noise series was convoluted using a Gaussian waveform of constant (0.2 or 0.7 nm) width, then renormalized and added to the original white noise series. Vogel et al. (2013) propose the creation of synthetic spectra that include triangular noise based on low-pass binomial filtering. In doing so, they build on the work of Jähne (2005). To create the triangular noise, ten iterations of a low-pass binomial filter were applied to each series and this filtered noise was scaled to σ=1E-4. Separately, fifty iterations of the low-pass binomial filter were applied to the white noise and the output again scaled. All final noise spectra were renormalized to RMS 1E-4. Triangular noise was used in most synthetic spectra experiments.

The range over which spectra are examined influences the accuracy of spectral fit, so wavelength range sensitivity studies were conducted using the following algorithm. Individual spectra were analyzed multiple times following the procedures described by Vogel et al. (2013). The upper and lower limits of the spectral range used for analysis were systematically varied for all spectral fit intervals spanning between 2.5 nm and 40 nm in the range 430-470 nm using interval steps of 0.5 nm, and deviations from the known concentration were determined in terms of parts per trillion (ppt). A large number of mathematically valid ranges may be identified, though only a subset of these ranges is analytically meaningful. Within the analytical region, deviations from entered compound concentrations are low and the results are relatively insensitive to wavelength variance. Several wavelength ranges of particular interest were selected over which to compare the effects of altering variables. These ranges are the maximum

range (430-470 nm), a range including the full broad band centered at 454 nm (447-470 nm), and a range including the absorptions near 440 nm (430-447 nm). Finally, a stable wavelength region was identified using contour results and distributions of output concentrations determined for white, Gaussian, and triangular noise at 0.2 and 0.7 nm. The statistical analysis of retrievals shows that within a range of spectral fit intervals (lower wavelength 430-453 nm; upper wavelength 458-470 nm), the retrieved SCD was found stable within few percent. We determine the threshold at which a deviation from the known concentration is considered significant based on the variance observed in this area. Data is pooled from the eight noise scenarios to calculate the standard deviation in this area (N = 37,600 data points), and the 3σ level is defined as the threshold for significant difference.

This notation of the confidence in detection is largely independent of the signal-to-noise ratio. We have verified this by investigating a range of concentrations (2.3-223.6 ppt) of C12 and C13 glyoxal, with the total amount of glyoxal (C12 + C13) kept constant at 225.9 ppt (1E16 molecules cm^{-2} glyoxal SCD). Concentrations were derived from slant column density (SCD) units of molecules cm^{-2} assuming 18 km path length, which is typical for cavity-enhanced (CE) DOAS applications (Thalman and Volkamer 2010). The absolute deviation from the entered concentration for a given set of parameters remained constant across concentrations.

Table 1: Parameter testing of synthetic spectra, with triangular noise at 0.3 nm and 0^{th} order baseline correction unless otherwise indicated.

Parameter	Variations Considered for Case Studies
Resolution (nm)	0.2; 0.3; 0.4; 0.5; 0.6; 0.7; 1.5
Baseline correction order	0^{th}; 1^{st}; 2^{nd}; 3^{rd}; 4^{th}; 5^{th}
Cross sections	H_2O (5645 ppm); NO_2 (225.8 ppt); NO_2 (2258 ppt); H_2O (5645 ppm) and NO_2 (225.8 ppt); H_2O (5645 ppm) and NO_2 (2258 ppt)
Noise Types (all tested at 0.2 and 0.7 nm)	White; Gaussian-convoluted to 0.2 nm; Gaussian-convoluted to 0.7 nm; triangular

Resolution, as well as concentration, affects signal to noise ratios and thus confidence in

data interpretation. In order to assess the impact of resolution on spectrum quality, the high-resolution C12 and C13 glyoxal spectra were added and then convoluted, using Gaussian waveforms, to experimentally typical ranges between 0.2 and 0.7 nm. An additional convolution was performed at a resolution of 1.5 nm to test the limits of low-resolution performance. Deviation from entered concentration values was assessed as a function of signal-to-noise ratio (Equation 2):

$$\frac{S}{N} = \frac{\text{Peak signal}}{\text{RMS Noise } (1\times10^{-4})} \quad (2)$$

Because the peak of the summed signal varied with both resolution and the concentrations of each species, every noise-concentration pair had a unique S/N.

Field and laboratory experiments require simultaneous measurement of multiple atmospheric gases. To model the presence of other compounds, experimentally typical concentrations of water and NO_2 were introduced to synthetic spectra series at 0.3 nm resolution (Table 1). Water is highly abundant in the atmosphere while the abundance of NO_2 is variable, both trace gases absorb in the same spectral region as glyoxal. Spectra were derived from the NO_2 cross section (294 K) of Vandaele et al. (1998) and from the H_2O HITRAN cross section (Rothman et al. 2005). The synthetic spectra were then analyzed to test whether adding these additional absorbers to a DOAS analysis would change detected glyoxal concentrations.

Software analysis parameters can also impact detected concentrations. Within Windoas, a polynomial corrects for baseline drift, but because the cross sections used here are baseline-corrected a 0^{th}-order polynomial was generally used. All available polynomial degrees (0^{th}- 5^{th} order) were investigated at 0.3 nm resolution. It was hypothesized that higher levels of correction would not produce a significant change in deviation.

Safety Considerations

During the synthesis of glyoxal in a manifold, addition of oxygen after the addition of acetylene may lead to ignition of the gas mixture. To avoid ignition, the gas mixture was kinetically buffered with ~200 torr nitrogen in between the addition of acetylene and the addition of oxygen.

Results and Discussion

The background- and lamp-drift-corrected high-resolution absorption spectra are shown in Figure 3. These spectra are 1cm^{-1} optical resolution and were acquired over a five-hour collection period to reduce noise. The absorption spectra are calibrated to match the integral absorption reported in the V05 spectrum, which is shown for comparison. The correlation in the line positions of the rich ro-vibronic structure at visible wavelengths is excellent (Figure 3).

The use of a light-emitting diode in spectrum collection had several analytical advantages over alternative light sources. Partially as a result of beam directionality, the LED produces more useable photons than a Xe-arc lamp at visible wavelengths (Thalman and Volkamer 2010). The signal-to-noise ratio is increased by the greater number of photons, which decreases shot noise. The signal-to-noise ratio SNR_σ is also inversely proportional to the number of points N in a spectrum. For a given resolution, the point spacing is fixed, so increasing the signal-to-noise ratio requires reducing the bandwidth and examining narrower bandpasses:

$$SNR_\sigma = \sqrt{\frac{2}{N}} \times \frac{B(\sigma)}{B_{mean}} \times SNR_x \quad (3)$$

Here, $B(\sigma)$ is the signal at the wavelength of interest and B_{mean} is the mean spectral signal. The interferogram noise SNR_x is constant for a given instrument optical setup. The increase in signal-to-noise levels, especially at high resolutions, is a principal advantage of diodes over halogen lamps (Bhosale 2011). Although the temperature-stabilized LED did not eliminate the need for baseline drift correction, LED light sources are more stable than halogen light sources, which

contain peaks that vary in shape and intensity with gas temperature and pressure (Volkamer and Thalman 2010) over a given time period. Volkamer and Thalman (2010) report blue LED drift of, at most, 5×10^{-4} (optical density units), or under 1%, in 3 hours. In contract, a xenon arc lamp may drift by up to 5.4% below 30,000 cm^{-1} (Volkamer et al. 2005b) or 20% above 30,000 cm^{-1} (Voigt et al. 2002).

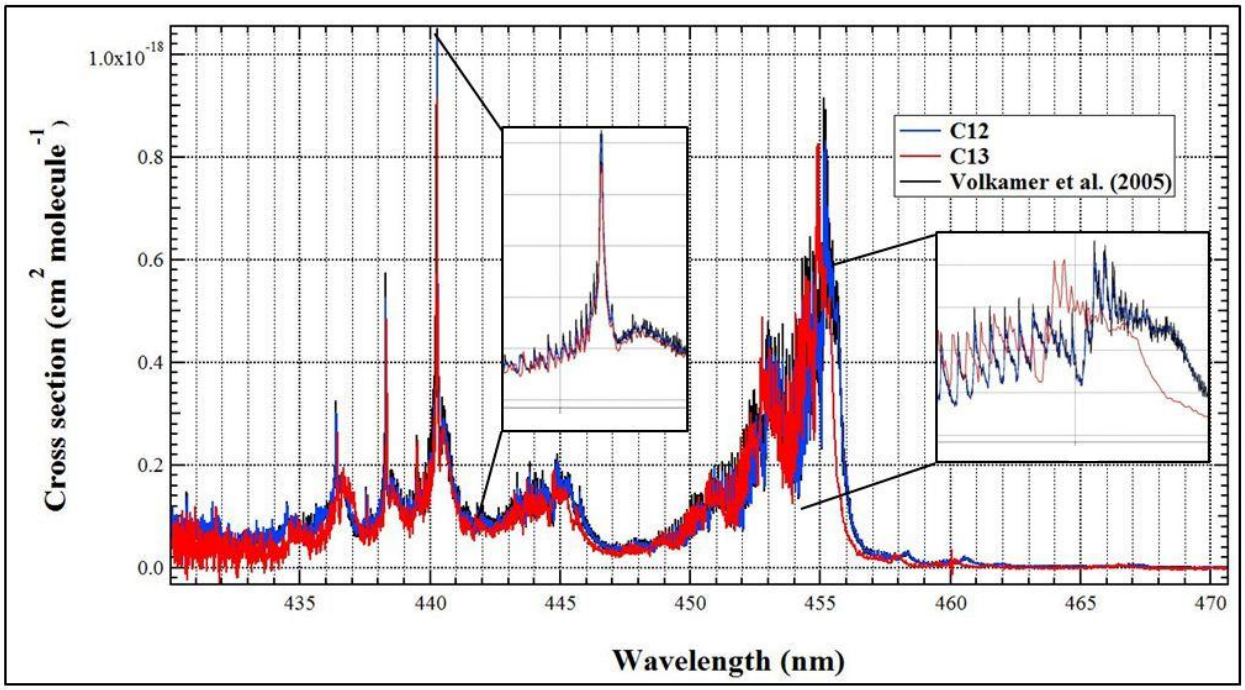

Figure 3: The C13 absorption cross section of C13 (red) is shifted near 455nm compared to C12 glyoxal (blue). Measured spectra are compared to the C12 high-resolution literature spectrum by Volkamer et al. (2005) (black).

The C12 glyoxal originates from acetylene that contains C13 in its natural 1.109% abundance. Disubstituted C13 glyoxal is hence expected to contribute in the C12 spectrum with an abundance of $(1.109\%)^2$, or 0.012%, which is below the detection limit for any S/N ratio <100. In this work, synthetic spectrum S/N ratios ranged between 62.6 and 40.5. Contamination of even C13-monosubstituted glyoxal is not significant as a source of error at the S/N levels explored here, but may require correction at higher S/N.

Non-uniform isotopic shifts were observed at peaks in both the corrected and in the

uncorrected spectra (Table 2). When different energetic transitions occur, the extent of any isotopic shift is dictated by symmetry elements and the involvement of carbon in a particular ro-vibrational motion. The variability of the shift, and even its disappearance at 440 nm, lends added importance to the decision of wavelength range selection for DOAS retrievals. The spectra are also relevant to the analysis of glyoxal term levels and symmetry (Birss et al., 1970; 1977), which is beyond the scope of this thesis. We can determine, though, that the isotopic shift in the upper electronic state is much smaller than in the ground state.

Table 2: C13-substitution shifts of some major peaks in the glyoxal cross section

	nm	cm^{-1}	nm	cm^{-1}	nm	cm^{-1}	nm	cm^{-1}	nm	cm^{-1}
C12	436.386	22915.5	440.267	22713.5	444.903	22476.8	453.018	22074.2	455.145	21971.0
C13	436.441	22912.6	440.257	22714.0	444.761	22484.0	452.761	22086.7	454.856	21985.0
Difference (C12-C13)	-0.055	3.1	0.010	0.5	0.142	-7.2	0.257	-12.5	0.289	-14

The assumption of selective DOAS detection is supported by tests of synthetic spectra such as the spectrum shown in Figure 4.

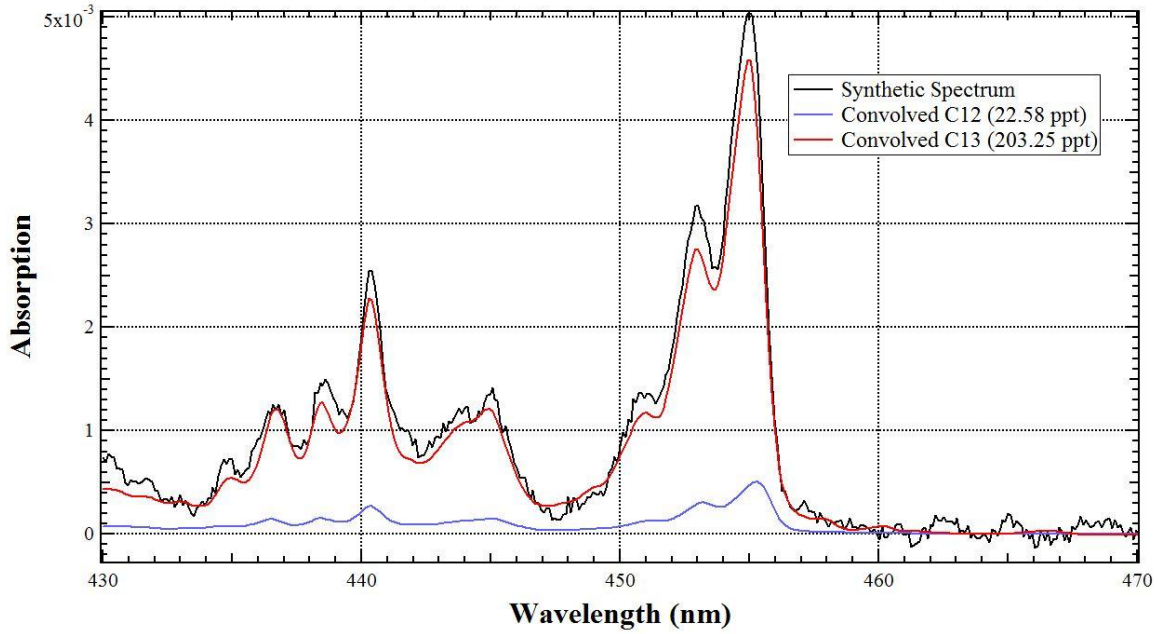

Figure 4: Synthetic spectrum at 0.7 nm resolution containing C12 (22.58 ppt) and C13 (203.25 ppt) glyoxal with triangular noise at RMS = 1E-4. The convolved data series that sum to create the synthetic spectrum signal are shown for comparison.

Decreasing resolution caused a linear increase in percent deviation from entered concentration ($R^2 > 0.95$ for all ranges and concentrations). Convolution to coarser resolution tends to flatten spectral peaks during smoothing, decreasing the signal-to-noise ratio through the use of broader Gaussian line functions (Figure 5).

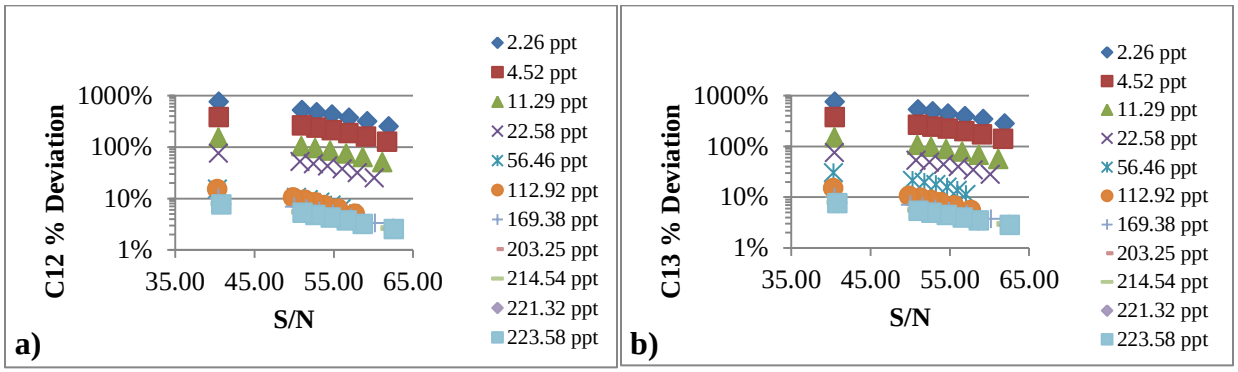

Figure 5: Linear increases in deviation with decreasing signal-to-noise for a) C12 and b) C13 under triangular noise conditions.

Detected glyoxal concentrations did not show a trend under changing baseline polynomial correction order.

Adding atmospheric concentrations of H_2O (Table 1) to a 0.3 nm resolution triangular noise spectrum changed detected C12 and C13 concentrations by less than one standard deviation over the 430-470 nm range. However, adding either concentration of NO_2 changed them by 11.3 ppt for a 50/50 C12/C13 mixing ratio, barely less than the 3σ significance criterion. H_2O does not absorb strongly in the range of peak glyoxal absorption (450-456 nm), while NO_2 absorbs strongly in that range. In analyses containing NO_2, C13 outputs had deviated upwardly from the input concentrations and became still higher as a result; C12 outputs deviated downwards and became a lower. The overall glyoxal SCD was thus changed slightly by introducing NO_2 because deviations were of similar, but not identical, magnitude and opposite sign. The more important effect of NO_2 addition is increased crosstalk between C12 and C13

spectra.

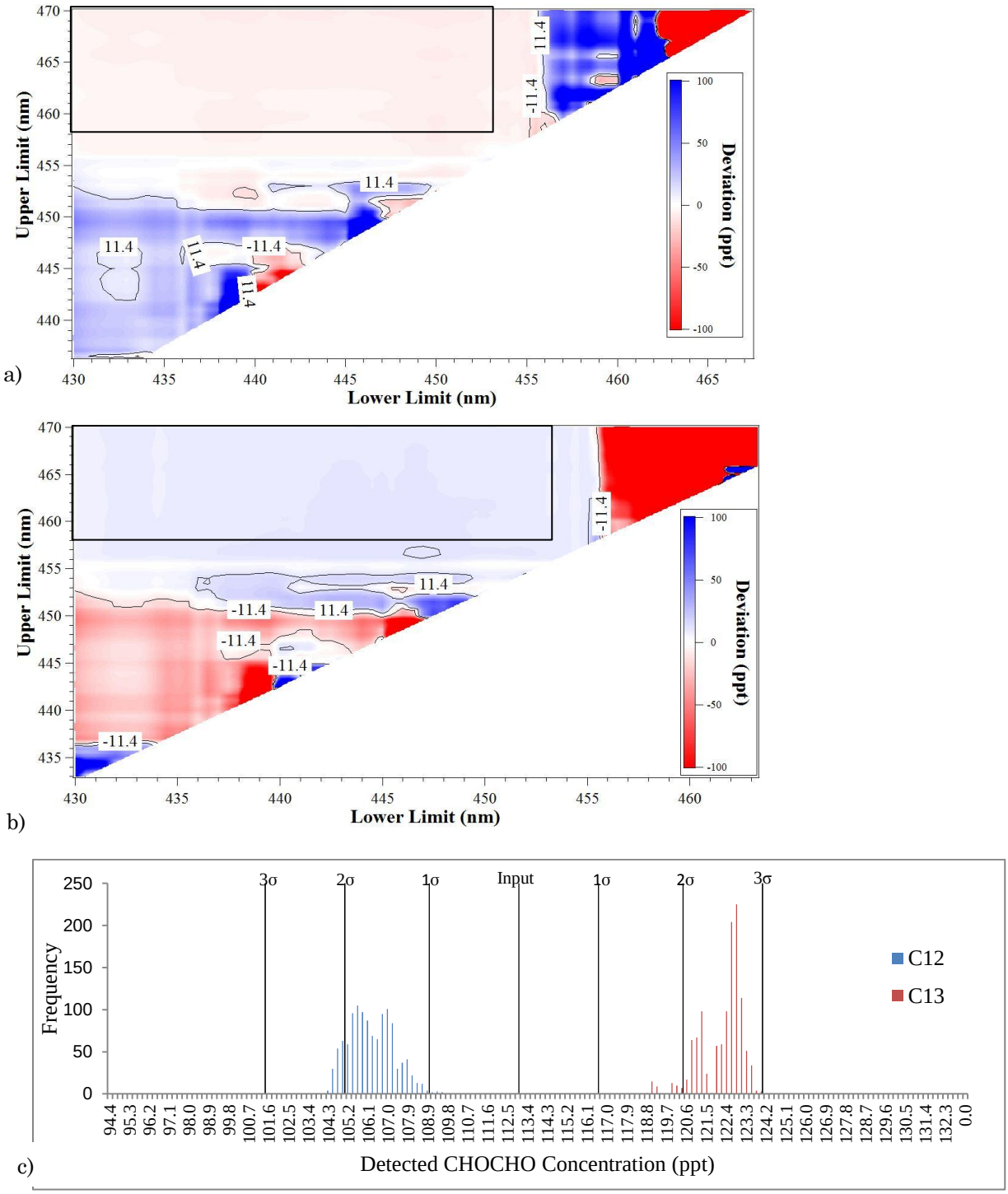

Figure 6: Sensitivity tests using synthetic spectra with triangular noise to assess the stability of typical DOAS retrievals. The deviation from known values is shown for: (panel A) C12 in a spectrum at 0.2 nm resolution containing 112.8 ppt C12 and 112.8 ppt C13; contour lines indicate the ±3σ significance bounds (see text). (B) C13 in that same spectrum. (C) Histogram of concentration output values in the wavelength-insensitive output range outlined by the boxed area in (A).

Finally, we find that the statistical noise which underlies procedures to introduce systematic noise can have a significant influence on data interpretation. The two different white noise spectra, A and B, interact differently with the synthetic spectra despite being produced using the same method. Deviations in the 430-470 nm range are smallest, followed by the 447-470 nm range and then the 430-447 nm range. While Noise A produced deviations 3.3-4.5 times smaller than the binomial filter method when convoluted to 0.2 nm, Noise B produced deviations 1.4-3.7 times larger. For a given series of spectra, C12 and C13 deviations always have opposite signs and nearly identical magnitudes.

Within the set of stable wavelength ranges shown in Figure 6 (see box in panels A and B), the global significance threshold is crossed by at least some noise spectra. A global significance threshold of $3\sigma = 11.4$ ppt was derived from the noise standard deviation of 1E-4 and from the average of all standard deviation values in C12 and C13 for all noise analyses (A and B) within that region. That rectangular grid is formed by a beginning wavelength of 430-453 nm and an ending wavelength of 458 to 470 nm. In total, 1176 ranges are contained within the stable region of each spectrum. Using a single noise spectrum would underestimate experimental variance because noise structure is unknown in ambient measurements. By considering the eight cases in building global statistics, a closer approximation is made to ambient conditions. The 0.2 nm and 0.7 nm triangular noise spectra differed significantly ($p<0.05$) (Table 3). In contrast, the 0.7 nm white noise spectra and the 0.7 nm resolution Gaussian (0.2 nm) spectra are not significantly different from each other.

Table 3: t-test results for different resolution and noise valued in synthetic spectra; p-values indicating significance are red.

	0.2 W	0.7 W	0.2 G2	0.7 G2	0.2 G7	0.7 G7	0.2 T	0.7 T
0.2 W	----------							

0.7 W	0.1111	----------						
0.2 G2	0.0391	0.3723	----------					
0.7 G2	0.0166	0.8996	0.0093	----------				
0.2 G7	0.0048	0.9783	0.0046	0.4287	----------			
0.7 G7	0.0186	0.1805	0.0154	0.0281	0.0493	----------		
0.2 T	0.0007	0.3580	0.6501	0.1218	0.0727	0.0436	----------	
0.7 T	0.0007	0.3848	0.0253	0.3694	0.1564	0.2728	0.0012	----------
Legend: 0.2 = convolution to 0.2 nm; 0.7 = convolution to 0.7 nm; W = white noise; G2 = Noise convoluted (Gaussian conv.) to 0.2 nm; G7 = Noise convoluted (Gaussian conv.) to 0.7 nm; T = triangular noise.								

Conclusions

Visible absorption spectra of both normal and C13 glyoxal were generated using the reaction of chlorine atoms with acetylene in air. The analysis of C12 and disubstituted C13 glyoxal spectra present in the same analytical environment produces significant and accurate outputs for each spectrum in the >10 ppt range for a range of standard resolutions and noise conditions. The spectra remain differentiable over a range of visible wavelengths encompassing the 455 nm strong-band absorption. Introduction of differing noise types provides a more accurate picture of noise conditions that could be encountered in ambient measurements. Inclusion of NO_2 absorptions, which are located at similar wavelengths, in synthetic spectra caused small perturbations in the overall amount of glyoxal detected while changing by ~10% the amounts of C12 and C13 glyoxal detected.

References

Atkinson, R. Atmospheric chemistry of VOCs and NO_x. *Atmos. Environ.* **2000,** *34,* 2063–2101.

Barros, A.; Rodrigues, J.A.; Almeida, P.J.; Oliva-Teles, M.T. Determination of glyoxal, methylglyoxal, and diacetyl in selected beer and wine, by HPLC with UV spectrophotometric detection, after derivatization with o-phenylenediamine. *J. Liquid Chromatogr. Relat. Technol.* **1999,** *22,* 2061-2069.

Bhosale, J.S. High signal-to-noise Fourier transform spectroscopy with light emitting diode sources. *Rev. Sci. Instrum.* **2011,** *82,* 093103.

Birss, F.W; Brown, J.M.; Cole, A.R.H.; Lofthuss, A.; Krishnamachari, L.N.G.; Osborne, G.A.; Paldus, J.; Ramsay, D.A.; Watmann., L. The 4550 Å band system of glyoxal. II. Vibration-rotational analyses for 12 bands of $C_2H_2O_2$. *Can. J. Phys.* **1970,** *48,* 1230-1241.

Birss, F.W.; Braund, D.B.; Cole, A.R.H.; Engleman Jr., R.; Green, A.A.; Japar, S.M.; Nanes, R.; Orr, B.J.; Ramsay, D.A.; Szyszka, S. The 4550 Å band system of glyoxal. IV. Vibration–rotational analyses for 11 bands of $^{13}C_2H_2O_2$ and determination of molecular geometries. *Can. J. Phys.* **1977,** *55,* 390–395.

Chen, Y.; Zhu, L. Wavelength-Dependent Photolysis of Glyoxal in the 290−420 nm Region. *Jour. Phys. Chem. A.* **2003,** *23,* 4643-4651.

Galloway, M.M.; Huisman, A.J.; Yee, L.D.; Chan, A.W.H.; Loza, C.L.; Seinfeld, J.H.; Keutsch, F.N. Yields of oxidized volatile organic compounds during the OH radical initiated oxidation of isoprene, methyl vinyl ketone, and methacrolein under high-NO_x conditions. *Atmos. Chem. Phys.* **2011,** *11,* 10779-10790.

Garcia, A.R.; Volkamer, R.; Molina, L.T.; Molina, M.J.; Samuelson, J.; Mellqvist, J.; Galle, B.; Herndon, S.C.; Kolb, C.E. Separation of emitted and photochemical formaldehyde in Mexico City using a statistical analysis and a new pair of gas-phase tracers. *Atmos. Chem. Phys.* **2006,** *6,* 4545-4557.

Grosjean D.; Grosjean E.; Gertler A.W. On-Road Emissions of Carbonyls from Light-Duty and Heavy-Duty Vehicles. *Environ. Sci. Technol.* **2001,** *35,* 45-53.

Jähne, B. *Digital Image Processing*; Springer, 2005, pp. 306–312.

Kielhorn, J., et al. Concise International Chemical Assessment Document 57: Glyoxal. World

Health Organization, 2004.

Larsen, R.W., Pawlowski, F.; Hegelund, F.; Jørgensen, P.; Gauss, J.; Nelander, B. The equilibrium structure of trans-glyoxal from experimental rotational constants and calculated vibration–rotation interaction constants. *Phys. Chem. Chem. Phys.* **2003,** *5,* 5031–5037.

Orlando, J; Tyndall, G. The atmospheric chemistry of the HC(O)CO radical. *Int. Jour. Chem. Kin.* **2001,** *33,* 149-156.

Plum, C. N.; Sanhueza, E.; Atkinson, R.; Carter, W. P. L.; Pitts, J.N. OH radical rate constants and photolysis rates of alpha-dicarbonyls, *Environ. Sci. Technol.* **1983**, *17,* 479 – 484.

Rothman, L. S., Jacquemart, D., Barbe, A., Benner, D. C., Birk, M., Brown, L. R., Carleer, M. R., Chackerian, C., Chance, K., Coudert, L. H., Dana, V., Devi, V. M., Flaud, J.-M., Gamache, R. R., Goldman, A., Hartmann, J.-M., Jucks, K. W., Maki, A. G., Mandin, J.-Y., Massie, S. T., Orphal, J., Perrin, A., Rinsland, C. P., Smith, M. A. H., Tennyson, J., Tolchenov, R. N., Toth, R. A., Vander Auwera, J., Varanasi, P., and Wagner, G.: The HITRAN 2004 molecular spectroscopic database. *J. Quant. Spectrosc. RA.* **2005,** *96,* 139–204.

Sinreich, R.; Coburn, S.; Dix, B.; Volkamer, R. Ship-based detection of glyoxal over the remote tropical Pacific Ocean. *Atmos. Chem. Phys.* **2010,** *10,* 11359–11371.

Stavrakou, T.; Muller, J.-F.; De Smedt, I.; Van Roozendael, M.; Kanakidou, M.; Vrekoussis, M.; Wittrock, F.; Richter, A.; Burrows, J. P. The continental source of glyoxal estimated by the synergistic use of spaceborne measurements and inverse modeling. *Atmos. Chem. Phys.* **2009,** *9,* 8431–8446.

Thalman, R.; Volkamer, R. Inherent calibration of a blue LED-CE-DOAS instrument to measure

iodine oxide, glyoxal, methyl glyoxal, nitrogen dioxide, water vapour and aerosol extinction in open cavity mode. *Atmos. Meas. Tech.* **2010,** *3,* 1797-1814.

Vandaele, A. C.; Hermans, C.; Simon, P. C.; Carleer, M.; Colin, R.; Fally, S.; Mèrienne, M.-F.; Jenouvrier, A.; Coquart, B. Measurements of the NO2 absorption cross-section from 42,000 cm-1 to 10,000 cm-1 (238–1000 nm) at 220 K and 294 K. *J. Quant. Spectrosc. Radiat. Transfer*. **1998,** *59,* 171-184.

Voigt, S.; Orphal, J.; Burrows, J.P. The temperature and pressure dependence of the absorption cross-sections of NO2 in the 250–800 nm region measured by Fourier-transform spectroscopy.

Vogel, L.; Sihler, H.; Lampel, J.; Wagner, T.; Platt, U. Retrieval interval mapping: a tool to visualize the impact of the spectral retrieval range on differential optical absorption spectroscopy evaluations. *Atmos. Meas. Tech.* **2013,** *6,* 275-299.

Volkamer, R.; Platt, U.; Wirtz, K. Primary and Secondary Glyoxal Formation from Aromatics: Experimental Evidence for the Bicycloalkyl−Radical Pathway from Benzene, Toluene, and p-Xylene. *J. Phys. Chem. A,* **2001,** *105,* 7865–7874.

Volkamer, R.; Molina, L.T.; Molina, M.J.; Shirley, T.; Brune, W.H.; DOAS measurement of Glyoxal as a new marker for fast VOC chemistry in urban air. *Geophys. Res. Lett.* **2005a,** *32,* L08806.

Volkamer, R.; Spietz, P; Burrows, J.; Platt, U. High-resolution absorption cross-section of glyoxal in the UV–vis and IR spectral ranges. *J. Photochem. Photobiol. A: Chem.* **2005b,** *172,* 35–46.

Volkamer, R.; San Martini, F.; Salcedo, D.; Molina, L. T.; Jimenez, J. L.; Molina, M. J. A Missing Sink for Gas-Phase Glyoxal in Mexico City: Formation of Secondary Organic Aerosol. *Geophys. Res. Lett.* **2007,** *34,* L19807.

Yamaguchi, M.; Ishida, J.; Zhu, X.X.; Nakamura, M.; Yoshitake, T. Determination of Glyoxal, Methylglyoxal, Diacethyl, and 2, 3-Pentanedione in Fermented Foods by High-Performance Liquid Chromatography with Fluorescence Detection. *J. Liquid Chromatogr*. ***1994,*** *17,* 203-211.

Yarwood, G; Peng, N.; Niki, H. FTIR study of the mechanism of the chlorine and bromine atom initiated oxidation of acetylene. *J. Phys. Chem.* **1991,** *95,* 7330-7337.